

First-principles study of magnetism, structure and chemical order in small FeRh alloy clusters

Junais Habeeb Mokkath and G. M. Pastor

Institut für Theoretische Physik, Universität Kassel,

Heinrich Plett Straße 40, 34132 Kassel, Germany

(Dated: October 13, 2021)

Abstract

The structural, electronic and magnetic properties of small Fe_mRh_n clusters having $N = m + n \leq 8$ atoms are studied in the framework of a generalized-gradient approximation to density-functional theory. The correlation between structure, chemical order, and magnetic behavior is analyzed as a function of size and composition. For $N = m + n \leq 6$ a thorough sampling of all cluster topologies has been performed, while for $N = 7$ and 8 only a few representative topologies are considered. In all cases the entire concentration range is systematically investigated. All the clusters show ferromagnetic-like order in the optimized structures. As a result, the average magnetic moment per atom $\bar{\mu}_N$ increases monotonously, which is almost linear over a wide range of concentration with Fe content. A remarkable enhancement of the local Fe moments beyond $3 \mu_B$ is observed as result of Rh doping. This is a consequence of the increase in the number of Fe d holes, due to charge transfer from Fe to Rh, combined with the extremely reduced local coordination. The Rh local moments, which are important already in the pure clusters ($N \leq 8$) are not significantly enhanced by Fe doping. However, the overall stability of magnetism, as measured by the energy gained upon spin polarization, increases when Rh is replaced by Fe. The composition dependence of the electronic structure and the influence of spin-orbit interactions on the cluster stability are discussed.

PACS numbers: 75.75.+a, 36.40.Cg, 75.50.Bb, 73.22.-f

I. INTRODUCTION

Alloying elements with complementary qualities in order to tailor their physical behavior for specific technological purposes has been a major route in material development since the antiquity. Cluster research is no exception to this trend. After decades of systematic studies of the size and structural dependence of the most wide variety of properties of mono-element particles, the interest has actually been moving progressively over the past years towards investigations on finite-size binary alloys.¹ The magnetism of transition-metal (TM) clusters opens numerous possibilities and challenges in this context.²⁻¹⁷ For example, one would like to understand how to modify the magnetic characteristics of clusters, in particular the saturation magnetization and the magnetic anisotropy energy (MAE), as it has been done in solids. This would indeed allow one to design new nanostructured materials from a microscopic perspective. Nevertheless, it is also true that controlling composition, system size, and magnetic behavior sets serious difficulties for both experiment and theory.

Pure TM clusters such as Fe_N , Co_N and Ni_N show spin moments, orbital moments, and MAEs that are enhanced with respect to the corresponding periodic solids.¹⁸⁻²⁴ Still, the possibilities of optimizing the cluster magnetic behavior by simply tuning the system size have been rather disappointing, particularly concerning the MAE, which remains relatively small—despite being orders of magnitude larger than in solids²¹—due to the rather weak spin-orbit (SO) coupling in the $3d$ atoms. This is one of the motivations for alloying $3d$ TMs with $4d$ and $5d$ elements which, being heavier, are subject to stronger SO interactions. In this context it is useful to recall that large nanoparticles and three dimensional solids of these elements are non-magnetic. However, at very small sizes the $4d$ and $5d$ clusters often develop a finite spontaneous low-temperature magnetization, due to the reduction of local coordination and the resulting d -band narrowing.²⁵⁻²⁹ The first experimental observation of this important finite-size effect has been made by Cox *et al.* by performing Stern-Gerlach-deflection measurements on Rh_N clusters. In this work the average magnetic moments per atom $\bar{\mu}_N = 0.15\text{--}0.80\mu_B$ have been experimentally determined for $N \leq 30\text{--}50$ atoms.²⁷ In view of these contrasting features one expects that $3d\text{--}4d$ and $3d\text{--}5d$ alloy clusters should show very interesting structural, electronic and magnetic behaviors.

The purpose of this paper is to investigate the ground-state properties of the small FeRh clusters in the framework of Hohenberg-Kohn-Sham's density functional theory.³⁰ Besides

the general interest of the problem from the perspective of $3d$ - $4d$ nanomagnetism, these clusters are particularly appealing because of the remarkable phase diagram of FeRh bulk alloys.³¹ In the case of Fe₅₀Rh₅₀ the magnetic order at normal pressure and low temperatures is antiferromagnetic (AF). As the temperature increases this α'' phase undergoes a first order transition to a ferromagnetic (FM) state, the α' phase, which is accompanied by a change in lattice parameter. The corresponding transition temperature $T_c^{\alpha'\alpha''}$ increases rapidly with increasing external pressure P , eventually displacing the FM α' phase completely for $P \geq 7$ GPa ($T_c^{\alpha'\alpha''} \simeq 290K$ for Fe₅₀Rh₅₀ at normal pressure). Moreover, $T_c^{\alpha'\alpha''}$ decreases very rapidly with decreasing Rh content. At low pressures the FM α' phase undergoes a FM to paramagnetic (PM) transition at ($T_C \simeq 670K$).³¹ In addition, the properties of α -FeRh bulk alloys have been the subject of first principles and model theoretical investigations.³² In particular these show that the relative stability of the FM and AF solutions depends strongly on the interatomic distances. Such remarkable condensed-matter effects enhance the appeal of small FeRh particles as specific example of $3d$ - $4d$ nanoscale alloy. Investigations of their magnetic properties as a function of size, composition, and structure are therefore of fundamental importance.

The remainder of the paper is organized as follows. In Sec. II the main details of the theoretical background and computational procedure are presented. This includes in particular a description of the strategy used for exploring the cluster energy landscape as a function of geometrical conformation and chemical order. The results of our calculations for FeRh clusters having $N \leq 8$ atoms are reported in Secs. III and IV. First, we focus on the interplay between structure, chemical order and magnetism in the most stable geometries for different cluster sizes. Second, we analyze the concentration dependence of the cohesive energy, the local and average magnetic moments, and the spin-polarized electronic structure. Finally, we conclude in Sec. V with a summary of the main trends and an outlook to future extensions.

II. COMPUTATIONAL ASPECTS

The calculations reported in this work have been performed in the framework of Hohenberg-Kohn-Sham's density functional theory,³⁰ as implemented in the Vienna ab initio simulation package (VASP).³³ The exchange and correlation energy is described by using both the spin-

polarized local density approximation (LDA) and Perdew and Wang’s generalized-gradient approximation (GGA).³⁴ The VASP solves the spin-polarized Kohn-Sham equations in an augmented plane-wave basis set, taking into account the core electrons within the projector augmented wave (PAW) method.³⁵ This is an efficient frozen-core all-electron approach which allows to incorporate the proper nodes of the Kohn-Sham orbitals in the core region and the resulting effects on the electronic structure, total energy and interatomic forces. The $4s$ and $3d$ orbitals of Fe, and the $5s$ and $4d$ orbitals of Rh are treated as valence states. The wave functions are expanded in a plane wave basis set with the kinetic energy cut-off $E_{max} = 268$ eV. In order to improve the convergence of the solution of the selfconsistent KS equations the discrete energy levels are broadened by using a Gaussian smearing $\sigma = 0.02$ eV. The validity of the present choice of computational parameters has been verified.³⁶ The PAW sphere radii for Fe and Rh are 1.302 Å and 1.402 Å, respectively. A simple cubic supercell is considered with the usual periodic boundary conditions. The linear size of the cell is $a = 10\text{--}22$ Å, so that any pair of images of the clusters are well separated and the interaction between them is negligible. Since we are interested in finite systems, the reciprocal space summations are restricted to the Γ point.

Although the potential advantages of alloying magnetic $3d$ elements with highly-polarizable $4d$ or $5d$ elements can be grasped straightforwardly, the problem involves a number of serious practical challenges. Different growth or synthesis conditions can lead to different chemical orders, which can be governed not just by energetic reasons but by kinetic processes as well. For instance, one may have to deal with segregated clusters having either a $4d$ core and a $3d$ outer shell or vice versa. Post-synthesis manipulations can induce different degrees of intermixing, including for example surface diffusion or disordered alloys. Moreover, the inter atomic distances are also expected to depend strongly on size and composition. Typical TM-cluster bond-lengths are in fact 10–20% smaller than in the corresponding bulk crystals. Taking into account that itinerant $3d$ -electron magnetism is most sensitive to the local and chemical environments of the atoms,^{26,37–39} it is clear that controlling the distribution of the elements within the cluster is crucial for understanding magnetic nanoalloys.

Systematic theoretical studies of binary-metal clusters are hindered by the diversity of geometrical conformations, ordered and disorder arrangements, as well as segregation tendencies that have to be taken into account. This poses a serious challenge to both first-principles and model approaches. In order to determine the interplay between cluster struc-

ture, chemical order and magnetism in FeRh clusters we have performed a comprehensive set of electronic calculations for clusters having $N \leq 8$ atoms. In the present paper we focus on the most stable cluster structure and magnetic configuration, which are determined by exploring the ground-state energy landscape.⁴⁰ This is a formidable task, since one needs to consider a large, most possibly complete and unbiased set of initial structures. Such a thorough geometry optimization must include not only the representative cluster geometries or topologies, but also all relevant chemical orders. This requires taking into account all distributions of the Fe and Rh atoms for any given size and composition. These two aspects of the problem of determining the structure of nanoalloys are discussed in more detail in the following.

The different cluster topologies are sampled by generating all possible graphs for $N \leq 6$ atoms as described in Ref. 38 (see also Ref. 41). For each graph or adjacency matrix it is important to verify that it can be represented by a true structure in $D \leq 3$ dimensions. A graph is acceptable as a cluster structure, only if a set of atomic coordinates \vec{R}_i with $i = 1, \dots, N$ exists, such that the interatomic distances R_{ij} satisfy the conditions $R_{ij} = R_0$ if the sites i and j are connected in the graph (i.e., if the adjacency matrix element $A_{ij} = 1$) and $R_{ij} > R_0$ otherwise (i.e., if $A_{ij} = 0$). Here R_0 refers to the nearest neighbor (NN) distance, which at this stage can be regarded as the unit of length, assuming for simplicity that it is the same for all clusters. Notice that for $N \leq 4$ all graphs are possible cluster structures. For example, for $N = 4$, the different structures are the tetrahedron, rhombus, square, star, triangular racket and linear chain.³⁸ However, for $N \geq 5$ there are graphs, i.e., topologies, which cannot be realized in practice. For instance, it is not possible to have five atoms being NNs from each other in a three dimensional space. Consequently, for $N \geq 5$ there are less real structures than mathematical graphs. The total number of graphs (structures) is 21 (20), 112 (104), and 853 (647) for $N = 5, 6$, and 7, respectively.³⁸

For clusters having $N \leq 6$ atoms all these topologies have indeed been taken as starting points of our structural relaxations. Out of this large number of different initial configurations the unconstrained relaxations using VASP lead to only a few geometries, which can be regarded as stable or metastable isomers. For larger clusters ($N = 7$ and 8) we do not aim at performing a full global optimization. Our purpose here is to explore the interplay between magnetism and chemical order as a function of composition for a few topologies that are representative of open and close-packed structures. Taking into account our results for

smaller sizes, and the available information on the structure of pure Fe_N and Rh_N clusters, we have restricted the set of starting topologies for the unconstrained relaxation of FeRh heptamers and octamers to the following: bicapped trigonal bipyramid, capped octahedra, and pentagonal bipyramid for $N = 7$, and tricapped trigonal bipyramid, bicapped octahedra, capped pentagonal bipyramid and cube for $N = 8$. Although, the choice of topologies for $N = 7$ and 8 is quite restricted, it includes compact as well as more open structures. Therefore, it is expected to shed light on the dependence of the magnetic properties on the chemical order and composition.

The dependence on concentration is investigated systematically for each topology of Fe_mRh_n by varying m and for each size $N = m + n \leq 8$, including the pure Fe_N and Rh_N limits. Moreover, we take into account all possible non-equivalent distributions of the m Fe and n Rh atoms within the cluster. In this way, any *a priori* assumption on the chemical order is avoided. Obviously, such an exhaustive combinatorial search increasingly complicates the computational task as we increase the cluster size, and as we move away from pure clusters towards alloys with equal concentrations. Finally, in order to perform the actual density-functional calculations we set for simplicity all NN distances in the starting cluster geometry equal to the Fe bulk value⁴² $R_0 = 2.48 \text{ \AA}$. Subsequently, a fully unconstrained geometry optimization is performed from first principles by using the VASP.³³ The atomic positions are fully relaxed by means of conjugate gradient or quasi-Newtonian methods, without imposing any symmetry constraints, until all the force components are smaller than the threshold 5 meV/\AA . The convergence criteria are set to 10^{-5} eV/\AA for the energy gradient, and $5 \times 10^{-4} \text{ \AA}$ for the atomic displacements.⁴³ The same procedure applies to all considered clusters regardless of composition, chemical order, or total magnetic moment. Notice that the diversity of geometrical structures and atomic arrangements often yields many local minima on the ground-state energy surface, which complicates significantly the location of the lowest-energy configuration.

Lattice structure and magnetic behavior are intimately related in TMs, particularly in weak ferromagnets such as Fe and its alloys.⁴⁴ On the one side, the optimum structure and chemical order depend on the actual magnetic state of the cluster as given by the average magnetic moment per atom $\bar{\mu}_N$ and the magnetic order. On the other side, the magnetic behavior is known to be different for different structures and concentrations. Therefore, in order to rigorously determine the ground-state magnetic properties of FeRh clusters, we have

varied systematically the value of the total spin polarization of the cluster S_z by performing fixed spin-moment (FSM) calculations in the whole physically relevant range. Let us recall that $S_z = (\nu_\uparrow - \nu_\downarrow)/2$ where $\nu_\uparrow(\nu_\downarrow)$ represents the number of electrons in the majority (minority) states. In practice we start from the non-magnetic state ($S_z^{min} = 0$) and increase S_z until the local spin moments are fully saturated, i.e., until the Fe moments in the PAW sphere reach $\mu_{Fe} \simeq 4\mu_B$ and the Rh moments $\mu_{Rh} \simeq 2.5\mu_B$ (typically, $S_z^{max} \gtrsim 3N/2$). The above described global geometry optimizations are performed independently for each value of S_z . These FSM study provides a wealth of information on the isomerization energies, the spin-excitation energies, and their interplay. These are particularly interesting for a subtle magnetic alloy such as FeRh, and would therefore deserve to be analyzed in some more detail. In the present paper we shall focus on the ground-state properties by determining for each considered Fe_mRh_n the most stable structural and magnetic configuration corresponding to energy minimum as a function of S_z and of the atomic positions.⁴⁰

Once the optimization with respect to structural and magnetic degrees of freedom is achieved, we derive the binding energy per atom $E_B = [mE(Fe) + nE(Rh) - E(Fe_mRh_n)]/N$ in the usual way by referring the total energy E to the corresponding energy of m Fe and n Rh isolated atoms. Moreover, for each stationary point of the total energy surface (i.e., for each relaxed structure having a nearly vanishing $\|\vec{\nabla}E\|$) we determine the vibrational frequencies from the diagonalization of the dynamical matrix. The latter is calculated from finite differences of the analytic gradients of the total energy. In this way we can rule out saddle points to which the local optimization procedure happens to converge on some occasions. Only configurations which correspond to true minima are discussed in the following. Finally, a number of electronic and magnetic properties—for example, the magnetic energy $\Delta E_m = E(S_z = 0) - E(S_z)$, the local magnetic moments μ_i integrated within the Wigner-Seitz (WS) or Bader atomic cells of atom i ,^{45,46} and the spin polarized density of electronic states (DOS) $\rho_\sigma(\varepsilon)$ —are derived from the self-consistent spin-polarized density and Kohn-Sham spectrum.

III. STRUCTURE AND MAGNETISM

In this section we discuss the ground-state structure, chemical order, binding energy, and magnetic moments of Fe_mRh_n clusters having $N = m + n \leq 8$ atoms. The main empha-




sis is here on understanding how the various electronic, structural and magnetic properties depend on the chemical composition of the alloy. First, each cluster size N is analyzed separately, since a strong dependence on N is expected in the small size, non-scalable regime. Comparisons between the various N are stressed by means of cross-references between different subsections. In addition the main trends as a function of size and concentration are summarized in Sec. IV.

A. FeRh dimers

Despite being the simplest possible systems, dimers allow to infer very useful trends on the relative strength, charge transfers and magnetic order in the various types of bonds which are found in FeRh alloy clusters. The results summarized in Table I show that the FeRh bond yields the highest cohesive energy, followed by the Rh₂ bond, the Fe₂ bond being the weakest. The particular strength of the heterogeneous bond is confirmed by the fact that the corresponding vibrational frequency is the highest. The bond length, however, follows the trend of the atomic radius which, being larger for Rh, gives $d_{\text{RhRh}} > d_{\text{FeRh}} > d_{\text{FeFe}}$. Quantitatively, the binding energy per atom $E_B^{\text{GGA}} = 1.35$ eV obtained for Fe₂ within the GGA is smaller than the LDA result $E_B^{\text{LDA}} = 2.25$ eV⁴⁸ although it still remains larger than the experimental value $E_B^{\text{expt}} = 0.65$ eV reported in Ref. 51. The calculated vibrational frequency $\nu_0(\text{Fe}_2) = 288$ cm⁻¹ is consistent with previous experimental results [$\nu_0(\text{Fe}_2) = 299.6$ cm⁻¹ from Ref. 51 and $\nu_0(\text{Fe}_2) = 300 \pm 15$ cm⁻¹ from Ref. 52]. Our result for E_B and $\bar{\mu}_N$ of Rh₂ coincide with previous GGA calculations by B. V. Reddy *et al.*⁵³ These are however larger than the experimental values $E_B^{\text{expt}}(\text{Rh}_2) = 1.46$ eV derived from Knudsen effusion,⁵⁶ $E_B^{\text{expt}}(\text{Rh}_2) = 0.70 \pm 0.15$ eV derived from resonance Raman in Ar matrices⁵⁷ and $E_B^{\text{expt}}(\text{Rh}_2) = 1.203$ eV derived from the resonant two-photon ionization.⁵⁸ The calculated vibrational frequency of $\nu_0(\text{Rh}_2)^{\text{GGA}} = 224$ cm⁻¹ should be compared with the experimental value $\nu_0(\text{Rh}_2)^{\text{expt}} = 283.9$ cm⁻¹ reported in Ref. 57.

The stability of magnetism, as measured by the difference in the total energy ΔE_m of the non-magnetic ($S_z = 0$) and optimal magnetic solutions, is largest for Fe₂ and smallest for Rh₂. The same trend holds for the average magnetic moment per atom which decreases linearly from $\bar{\mu}_2 = 3\mu_B$ to $2\mu_B$ as one goes from Fe₂, to FeRh, to Rh₂. These average magnetic moments per atom correspond to a full polarization of all d electrons in the WS

TABLE I. (Color online) Structural, electronic and magnetic properties of FeRh dimers. Results are given for the binding energy E_B (in eV), the magnetic stabilization energy $\Delta E_m = E(S_z = 0) - E(S_z)$ (in eV), the average interatomic distance $d_{\alpha\beta}$ (in Å) between atoms α and β ($\alpha, \beta = \text{Fe}$ or Rh), the average spin moment per atom $\bar{\mu}_N = 2S_z/N$ (in μ_B), the local spin moment μ_α (in μ_B) at the Fe or Rh atoms, and the vibrational frequency ν_0 (in cm^{-1}).

Cluster	Struct.	E_B	ΔE_m	$d_{\alpha\beta}$	$\bar{\mu}_N$	μ_{Fe}	μ_{Rh}	ν_0
Fe ₂		1.35	0.77	1.98	3.00	2.82		288
FeRh		1.95	0.24	2.07	2.50	3.34	1.33	359
Rh ₂		1.65	0.00	2.21	2.00		1.83	224

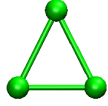
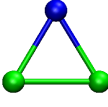
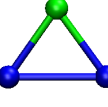
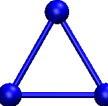
spheres: $\nu_d \simeq 7$ for Fe and $\nu_d \simeq 8$ for Rh, where ν_d stands for the number of valence d electrons of the corresponding atom. The local magnetic moments μ_α ($\alpha \equiv \text{Fe}$ and Rh), are obtained by integrating the spin density within the PAW spheres which have the radius $r_{\text{PAW}}(\text{Fe}) = 1.3 \text{ \AA}$ for Fe and $r_{\text{PAW}}(\text{Rh}) = 1.4 \text{ \AA}$ for Rh. In the pure dimers, the local moments $\mu_{\text{Fe}} = 2.82\mu_B$ and $\mu_{\text{Rh}} = 1.83\mu_B$ are close to the respective total moment per atom $\bar{\mu}_2 = 3\mu_B$ and $2\mu_B$, which indicates that the spin-density $m(\vec{r}) = n_\uparrow(\vec{r}) - n_\downarrow(\vec{r})$ is quite localized around the atoms. Actually, the differences between μ_α and $\bar{\mu}_N$ give a measure of the small spill-off effect in $m(\vec{r})$. Taking this into account, the results for μ_α in the FeRh dimer seem quite remarkable. Here the Fe local moment is significantly enhanced with respect to the Fe₂ or Fe-atom value, while the Rh moment is reduced by a similar amount ($\Delta\mu_{\text{Fe}} = 0.52 \mu_B$ and $\Delta\mu_{\text{Rh}} = -0.50 \mu_B$, see Table I). This is mainly the consequence of a transfer of d electrons from Fe to Rh, which allows the Fe atom to develop a larger spin moment, due to the larger number of d holes. This occurs at the expense of the moment at the Rh atom, which has less d holes to polarize. An integration of the electronic density in the Bader cells⁴⁵ shows that 0.33 electrons are transferred from the Fe to the Rh atom in FeRh. This behavior is qualitatively in agreement with the higher Pauling electronegativity χ of the Rh atom ($\chi_{\text{Fe}} = 1.83$ and $\chi_{\text{Rh}} = 2.28$).⁵⁹

B. FeRh trimers

The results for trimers are summarized in Table II. As expected, the lowest energy isomers are found to be triangles for all compositions. According to our calculations the ground state of Rh_3 is an equilateral triangle (D_{3h}) with $E_B = 2.31$ eV, bond length $d = 2.37$ Å and average magnetic moment $\bar{\mu}_3 = 1\mu_B$. The local magnetic moments $\mu_\alpha = 0.93\mu_B$ in the WS cells align parallel to each other and are almost as large as $\bar{\mu}_3$. These results are consistent with those reported in previous GGA studies of Rh_3 ($E_B = 2.35$ eV, $d = 2.45$ Å and $\bar{\mu}_3 = 1\mu_B$).⁵³ A single Fe substitution yields an isosceles FeRh_2 with an elongated base composed of the two Rh atoms. Notice that the bond-length $d_{\text{RhRh}} = 2.57$ Å is larger than in Rh_3 . The linear isomer of the form Rh-Fe-Rh, i.e., with only FeRh bonds, lies 0.4 eV above the optimal structure. It is the only true local minimum among the linear FeRh trimers. The other linear structures (Rh-Rh-Fe, Fe-Rh-Fe, and Fe-Fe-Rh) are all found to be saddle points connecting triangular minima of the potential energy surface (PES). Further Fe substitution yields a isosceles Fe_2Rh in which the FeFe bond is the shortest. One observes, as in the dimers, that the interatomic distances follow the trends in the atomic radii. Finally, for Fe_3 , the calculated lowest-energy structure is a Jahn-Teller distorted isosceles triangle with two longer bonds ($d_{12} = d_{13} = 2.30$ Å) and a shorter one ($d_{23} = 2.07$ Å). The calculated average magnetic moment of Fe_3 is $\bar{\mu}_3 = 3.33\mu_B$. These results coincide with previous GGA studies⁴⁷ predicting $d_{12} = d_{13} = 2.33$ Å and $d_{23} = 2.09$ Å. In contrast, LDA calculations⁴⁸ yield an equilateral Fe_3 with average magnetic moment $\bar{\mu}_3 = 2.66\mu_B$ and $d = 2.10$ Å. By using the spin-polarized LDA, we also obtain an equilateral triangle similar to the one reported in Ref. 48. In contrast, in the GGA one finds that the equilateral triangle (D_{3h}) is unstable with respect to a Jahn-Teller distortion. The isosceles shape of Fe_3 can therefore be interpreted as a consequence of exchange and correlation effects. Moreover, we have analyzed the GGA Kohn-Sham spectrum in the equilateral structure and found a high degeneracy at the Fermi energy, which is consistent with the interpretation that the distortion is triggered by a Jahn-Teller effect.

Concerning the composition dependence of E_B one observes a non-monotonous behavior as for $N = 2$, which indicates that the FeRh bonds are the strongest. The lowest vibrational frequency follows a similar trend, despite the larger mass of Rh. Notice that FeRh_2 is somewhat more stable than Fe_2Rh , since the bonds between Rh atoms are in general stronger

TABLE II. (Color online) Structural, electronic and magnetic properties of FeRh trimers. Results are given for the binding energy per atom E_B (in eV), the magnetic stabilization energy per atom $\Delta E_m = [E(S_z=0) - E(S_z)]/N$ (in eV), the average interatomic distance $d_{\alpha\beta}$ (in Å) ordered from top to bottom as d_{FeFe} , d_{FeRh} and d_{RhRh} , the average spin moment per atom $\bar{\mu}_N = 2S_z/N$ (in μ_B), the local spin moment μ_α (in μ_B) at the Fe or Rh atoms, and the lowest vibrational frequency ν_0 (in cm^{-1}).

Cluster	Struct.	E_B	ΔE_m	$d_{\alpha\beta}$	$\bar{\mu}_N$	μ_{Fe}	μ_{Rh}	ν_0
Fe ₃		1.80	0.69	2.22	3.33	2.99		267
Fe ₂ Rh		2.24	0.32	2.25 2.35	3.00	3.35	1.21	235
FeRh ₂		2.45	0.05	2.21 2.57	2.00	3.27	1.18	287
Rh ₃		2.31	0.02	2.37	1.00		0.93	210

than between Fe atoms. Finally, one may also notice that the energy gain ΔE_m associated to magnetism only plays a quantitative role in the relative stability of triangular and linear FeRh₂. ΔE_m is actually larger for the linear chain than for the triangle. Therefore, the later remains the most stable structure even in the non-magnetic case, although with somewhat different bond lengths.

The average magnetic moment per atom $\bar{\mu}_3$ amounts to $1\mu_B$ for Rh₃. In the alloys it increases monotonously with Fe doping, reaching $\bar{\mu}_3 = 10/3\mu_B$ for Fe₃. The local magnetic moments μ_α always show a FM-like coupling. They are all identical in Rh₃, which is consistent with the C_3 point-group symmetry. In the pure clusters μ_α is always close to $\bar{\mu}_3$. This indicates that the spin polarization is dominated by electrons occupying localized states and that spill-off contributions are not important. For example, in the case of Fe₃, one finds $\mu_1 = 3.23\mu_B$ and $\mu_2 = \mu_3 = 2.87\mu_B$, the latter corresponding to the pair of atoms forming the shorter bond. On the other side, the average local moments $\mu_{\text{Rh}} = 0.93\mu_B$ in Rh₃ should be compared with $\bar{\mu}(\text{Rh}_3) = 1\mu_B$. As soon as FeRh bonds are present, for


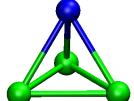
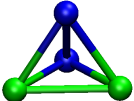
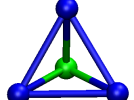
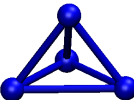
mixed compositions, the local Fe moments are enhanced beyond $3\mu_B$. This is mainly due to a charge transfer from Fe to Rh, leading to an increase in the number of Fe d holes as already observed in the dimer. Quantitatively, the local μ_{Fe} and μ_{Rh} in mixed trimers are similar, though somewhat smaller, to the corresponding values in the FeRh dimer. Notice, moreover, the enhancement of the Rh local moments in Fe_2Rh and FeRh_2 as compared to pure Rh_3 . This reflects the importance of the proximity of Fe on the magnetic behavior of the Rh atoms.

C. FeRh tetramers

The most stable FeRh tetramers are all tetrahedra and the first low-lying isomers are rhombi (see Table III). The distribution of the atoms within the optimal topology does not play a role since all sites are equivalent in a tetrahedron. In the case of Rh_4 we obtain a nonmagnetic undistorted tetrahedron having $E_B = 2.75$ eV and bond length $d = 2.45$ Å. The closest isomer is found to be a bent rhombus with an average bond length $d = 2.35$ Å. Similar results have been obtained in previous studies on Rh clusters.⁵⁴ Notice, however, that Bae *et al.*⁶² have obtained a bend rhombus as the ground-state structure for Rh_4 also by using VASP. This discrepancy is likely to be a consequence of the different choice of the pseudopotential and cutoff energy E_{max} . In our calculations we considered the PAW method and $E_{\text{max}} = 268$ eV, while in Ref. 62 one used ultrasoft pseudopotentials and $E_{\text{max}} = 205.5$ eV.

The binding energy of the alloys shows a characteristic non-monotonous dependence on concentration, which was also found in smaller clusters. In fact Fe_2Rh_2 and FeRh_3 are the most stable tetramers with $E_B = 2.74$ eV and $E_B = 2.76$ eV, respectively. This confirms that the FeRh bonds are the strongest. It is worth noting that these trends are not altered qualitatively if magnetism is neglected, i.e., if one considers E_B for $S_z = 0$. In addition, it is interesting to follow how E_B changes from Rh_4 to Fe_4 . The stability of the clusters can be qualitatively related to the number of homogeneous and heterogeneous bonds by counting them for each of the clusters shown in Table III. For instance, FeRh_3 , which is the most stable composition, has 3 FeRh and 3 RhRh bonds. Replacing a Rh by an Fe to obtain Fe_2Rh_2 implies replacing 2 RhRh bonds by a stronger FeRh and a weaker FeFe bond. Therefore, E_B does not change significantly. The fact that E_B depends weakly on

TABLE III. (Color online) Structural, electronic and magnetic properties of FeRh tetramers as in Table II.

Cluster	Struct.	E_B	ΔE_m	$d_{\alpha\beta}$	$\bar{\mu}_N$	μ_{Fe}	μ_{Rh}	ν_0
Fe ₄		2.21	0.35	2.28	3.50	3.08		279
Fe ₃ Rh		2.49	0.58	2.34 2.40	3.00	3.18	1.03	232
Fe ₂ Rh ₂		2.74	0.37	2.52 2.31 2.72	2.50	3.39	1.03	243
FeRh ₃		2.76	0.21	2.30 2.60	1.75	3.25	1.12	289
Rh ₄		2.75	0.00	2.45	0.00		0.00	201

composition for Rh rich tetramers shows that FeRh and RhRh bonds are comparably strong in these clusters.

Concerning the magnetic moments one observes an approximately linear dependence of $\bar{\mu}_N$ as a function of Fe content. In general, the substitution of a Rh by an Fe atom results in an increase of the total moment $2S_z$ by 3 or $4\mu_B$, or equivalently, $\Delta\bar{\mu}_N = (0.75-1)\mu_B$ (see Table III). The magnetic order is always FM-like. In the alloys the local moments μ_{Fe} show the above mentioned enhancement, which is due to a Fe-to-Rh d -electron charge transfer that increases the number of d holes and allows for the development of $\mu_{\text{Fe}} \simeq 3.2-3.4\mu_B$. In addition, the presence of Fe in Fe _{m} Rh _{n} enhances the Rh local moments as compared to pure Rh₄.

D. FeRh pentamers


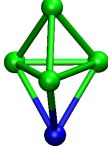
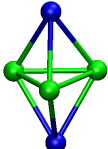
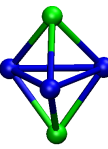
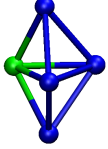
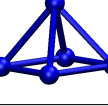
In Table IV the results for FeRh pentamers are summarized. Although all possible cluster topologies (20 structures) were considered as starting geometries for each composition, only the most highly coordinated trigonal bipyramid (TBP) and the square pyramid (SP) are

found to be most stable geometries. The low coordinated structures transform into compact structures after the relaxation. Except for Rh_5 , which optimal structure is a SP, all the other FeRh pentamers have the TBP as ground-state geometry. The trend in the composition dependence of the binding energy E_B of pentamers confirms the behavior we started to observe for $N = 4$. Indeed, in the Fe-rich limit E_B increases rapidly with increasing Rh content, as the weakest FeFe bonds are replaced by FeRh bonds. Later on, near 50% concentration and in the Rh-rich limit, the composition dependence is weak since FeRh and RhRh bonds are comparably strong (see Table IV). In particular for Rh-rich compositions, replacing Fe by Rh atoms no longer results in weaker binding. In other words, FeRh bonds are no longer primarily preferred. This is possibly a consequence of the increasing coordination number, which enhances the role of electron delocalization and band formation, thus favoring the larger Rh hybridizations.

The calculated optimal structure of Rh_5 , a square pyramid, coincides qualitatively with previous DFT calculations.⁵³ Nevertheless, we obtain a binding energy that is 0.07 eV per atom lower than in Ref. 53. Substituting one Rh atom by Fe yields FeRh_4 and changes the optimal cluster topology to the more compact TBP. The SP remains a local minimum of the ground-state energy surface, which is only 3 meV per atom less stable than the optimal TBP geometry. The average magnetic moment $\bar{\mu}(\text{FeRh}_4) = 1.2\mu_B$ is enhanced with respect to Rh_5 due to the contribution of a large Fe local moment $\mu_{\text{Fe}} = 3.31\mu_B$. Notice that the Rh moments are no longer enhanced as in the smaller FeRh_{N-1} but significantly reduced: $\mu_{\text{Rh}} = 0.62\mu_B$ for the apex atoms and $\mu_{\text{Rh}} = 0.52\mu_B$ for the Rh atoms sharing a triangle with the Fe. This is of course related to the fact that the ground-state S_z is relatively low. The effect is even stronger in the case of the SP isomer of FeRh_4 . Here we find two Rh moments $\mu_{\text{Rh}} = 0.43\mu_B$ that couple parallel to the Fe moment, one very small Rh local moment $\mu_{\text{Rh}} = 0.05\mu_B$, and an antiparallel moment $\mu_{\text{Rh}} = -0.48\mu_B$. This explains the reduced average total moment $\bar{\mu}_5 = 0.8\mu_B$ and the very small average Rh moment $\mu_{\text{Rh}} = 0.15\mu_B$ found in SP isomer of FeRh_4 . The present example illustrates the subtle competition between cluster structure and magnetism in $3d$ - $4d$ nanoalloys.

Further increase in the Fe content does not change the topology of the optimal structure. Moreover, we start to see that for nearly equal concentrations of Fe and Rh (i.e., Fe_2Rh_3 and Fe_3Rh_2) the low-lying isomers are the result of changes on the chemical order, i.e., changes in the distribution of the Fe and Rh atoms within the cluster, rather than the result of changes

TABLE IV. (Color online) Structural, electronic and magnetic properties of FeRh pentamers as in Table II.

Cluster	Struct.	E_B	ΔE_m	$d_{\alpha\beta}$	$\bar{\mu}_N$	μ_{Fe}	μ_{Rh}	ν_0
Fe ₅		2.51	1.00	2.41	3.20	2.93		227
Fe ₄ Rh		2.76	1.01	2.30 2.47	3.00	3.09	1.06	243
Fe ₃ Rh ₂		2.96	0.92	2.37 2.39	2.40	3.13	0.75	244
Fe ₂ Rh ₃		3.06	0.55	2.35 2.71	2.20	3.36	1.08	260
Fe ₁ Rh ₄		3.01	0.33	2.39 2.51	1.20	3.31	0.57	251
Rh ₅		3.03	0.70	2.48	1.00		0.95	113

in the cluster topology. The most stable configuration corresponds to the case where the 3 Rh atoms (in Fe₂Rh₃) or the 3 Fe atoms (in Fe₃Rh₂) are all NNs of each other (see Table IV). This is understandable from a single-particle perspective, since the band energy is lower when orbitals having nearly the same energy levels are hybridized. In addition, the most stable configurations maximize first the number of FeRh NN pairs, followed by the number of RhRh pairs.⁶⁰ Finally, in the Fe-rich limit, for example in Fe₄Rh, the lowest-energy structure remains a TBP but the closest isomer corresponds to the SP, which has a different topology, rather than a different position of the Rh atom in the TBP.

The trends in the magnetic properties are dominated by the Fe content. As for smaller clusters the average magnetic moment per atom $\bar{\mu}_N$ increases monotonously with increasing

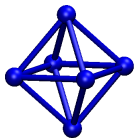
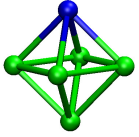
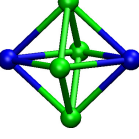
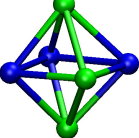
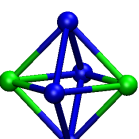
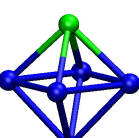
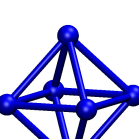
Fe concentration. This holds for all optimal structures and in most of the first excited isomers. In fact the latter show in general the same $\bar{\mu}_N$ as the optimal structure. The only exception is FeRh_4 , which is also the only case where an antiparallel alignment of Rh local moments is found. In all other investigated cases the magnetic order was found to be FM-like. The local Fe moments show the usual enhancement with respect to pure Fe_N , due to an increase in the number of Fe d -holes. This effect is stronger for Rh-rich clusters, since the larger the number of Rh atoms is, the stronger is the FeRh charge transfer (see Table IV). In contrast, the substitution of Rh by Fe does not always enhances the Rh local moments, as we observed systematically for smaller sizes. Finally, it is interesting to observe that the different chemical orders found in the low lying isomers of Fe_2Rh_3 and Fe_3Rh_2 correspond to different local magnetic moments. The environment dependence of μ_α follows in general the well-known trend of higher spin polarization at the lowest coordinated sites.

E. FeRh hexamers

In Table V the results for FeRh hexamers are summarized. For each composition all possible cluster topologies (63 different graphs^{38,41}) and all non-equivalent distributions of Fe and Rh atoms were taken into account as initial guess for the *ab initio* optimization of the cluster geometry. As in previous cases, all relevant values of the total magnetic moment $2S_z$ are scanned. Despite the diversity of starting topologies most low coordinated structures relax into compact ones in the course of the unconstrained relaxations. In the end, the square bipyramid (SBP), in general somehow slightly distorted, yields the lowest energy regardless of composition.

The binding energy per atom E_B shows a similar composition dependence as for pentamers. For Fe-rich clusters E_B increases steadily with increasing Rh content, by about 0.2 eV each time a Rh replaces an Fe (see Table V). Qualitatively, this confirms that the bonding between Fe and Rh is stronger than between Fe atoms. However, for nearly equal concentrations and in the Rh-rich clusters ($\text{Fe}_m\text{Rh}_{6-m}$ with $m \leq 2$) E_B becomes almost independent of m . This seems to be the result of a compensation of bonding and magnetic contributions. In fact, on the one side, the magnetic energy ΔE_m continues to decrease with increasing Rh content, by about 0.1–0.2 eV per Rh substitution, even for high Rh content. And on the other side, this is compensated by an increase of the bonding energy

TABLE V. (Color online) Structural, electronic and magnetic properties of FeRh hexamers as in Table II.

Cluster	Struct.	E_B	ΔE_m	$d_{\alpha\beta}$	$\bar{\mu}_N$	μ_{Fe}	μ_{Rh}	ν_0
Fe ₆		2.74	1.03	2.38	3.33	2.95		206
Fe ₅ Rh		2.94	1.07	2.38 2.46	3.16	3.10	1.20	210
Fe ₄ Rh ₂		3.14	0.85	2.38 2.45	3.00	3.28	1.22	214
Fe ₃ Rh ₃		3.21	0.56	2.62 2.38 2.61	2.50	3.32	1.14	239
Fe ₂ Rh ₄		3.26	0.38	2.46 2.51	2.33	3.38	1.39	207
FeRh ₅		3.24	0.28	2.44 2.54	1.83	3.37	1.33	192
Rh ₆		3.20	0.19	2.54	1.00		0.91	188

with increasing number of Rh atoms.

In the case of Rh₆ an octahedron with an average moment $\bar{\mu}_6 = 1\mu_B$ and average bond length $d = 2.54 \text{ \AA}$ yields the lowest energy. The first isomer, a trigonal bipyramid (TBP), lies only 28 meV above the optimum, showing a somewhat shorter average bond length $d = 2.46 \text{ \AA}$ and a higher average moment $\bar{\mu}_6 = 1.67\mu_B$. These results are consistent with previous DFT calculations.⁶¹ A single Fe substitution enhances the average moment to $\bar{\mu}_6 = 1.83\mu_B$ but does not change the topology of the optimal FeRh₅. The RhRh distances remain essentially unchanged and the FeRh distances are somewhat shorter. The important

increase in the ground-state spin polarization ($5\mu_B$ in all) is not only due to the larger Fe moment ($\mu_{\text{Fe}} = 3.37\mu_B$ in the PAW sphere) but also results from the enhancement of the local Rh moments ($\mu_{\text{Rh}} = 1.33\mu_B$, see Table V). The first isomer of FeRh_5 corresponds to a distorted trigonal prism with significantly contracted FeRh and RhRh bond lengths. In Fe_2Rh_4 the Fe atoms occupy the opposite apex positions of the octahedron. In this way each Fe is four-fold coordinated with all Rh atoms. Heterogeneous bonds are favored over FeFe ones. The local Fe moments in Fe_2Rh_4 are the largest among all hexamers: $\mu_{\text{Fe}} = 3.38\mu_B$, slightly beyond the value found in FeRh_5 . This corresponds to a large number of d holes. In addition, particularly important spin polarizations are induced at the neighboring Rh atoms ($\mu_{\text{Rh}} = 1.39\mu_B$). The first isomer of Fe_2Rh_4 corresponds to a capped trigonal bipyramid (CTBP) having a short FeFe NN bond. This structure lies only 0.11 eV higher in energy and has the same total moment as the optimal geometry. Replacing a further Fe atom yields Fe_3Rh_3 , whose optimal structure is an octahedron. Here we find two isosceles open Fe_3 and Rh_3 triangles that form a $\pi/2$ angle with respect to each other (see Table V). Out of the 12 NN pairs in the Fe_3Rh_3 octahedron, 8 are FeRh and only 4 are homogeneous (2 FeFe and 2 RhRh). The local Fe magnetic moments are similar to the other clusters but the Rh moments are somewhat smaller in average ($\mu_{\text{Rh}} = 1.14\mu_B$). The first excited isomer of Fe_3Rh_3 is a CTBP that lies 25 meV per atom above the ground state. The lowest-energy structure found for Fe_4Rh_2 is an octahedron, while a distorted CTBP is an isomer lying 0.14 eV per atom above. In the former the Rh atoms are far apart occupying the apical positions, whereas in the latter they are NNs. The situation is thus similar to what we find in Fe_3Rh_2 . For low Rh or Fe concentrations the atoms are distributed in order to favor the FeRh bonds rather than homogeneous NN pairs between the atoms in the minority. The octahedron and a distorted CTBP remain the two most stable structures as one further reduces the Rh content (see Table V for Fe_5Rh and Fe_6).

Concerning the magnetic properties one observes qualitatively similar trends as in the smaller clusters. The average magnetic moment per atom $\bar{\mu}_N$ increases monotonously with Fe content. Accordingly, the energy gain ΔE_m associated to magnetism also increases with the number of Fe atoms. There are in general very little differences in $\bar{\mu}_N$ between the optimal structure and the first low-lying isomer. The largest part of the spin polarization (about 90%) can be traced back to the local d magnetic moments with the PAW sphere of the atoms. As expected, the s and p spin polarizations are almost negligible in comparison

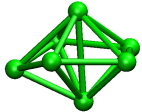
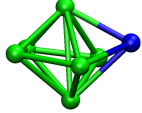
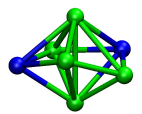
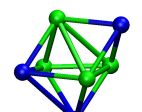
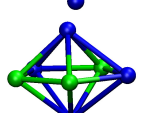
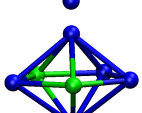
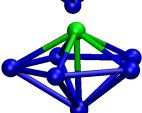
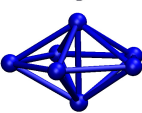
to the d -orbital contributions. A significant increase of the Fe moments is observed upon Rh doping, which result from the larger number of available Fe d holes and the low coordination number. Moreover, the Rh moments in Fe_mRh_n are stabilized by the proximity of the Fe atoms. In the alloy hexamers the values of μ_{Rh} are larger than in the pure Rh_6 . However, this is not a general trend, since the magnetic moments in small Rh_n are often quite important due to the extremely reduced coordination numbers.

F. Exploring heptamers and octamers

For Fe_mRh_n clusters having $m + n = N \geq 7$ we did not attempt to perform a systematic sampling of initial topologies for further unconstrained structural relaxation, as was done for the smaller sizes. Instead of aiming at a true global optimization, only a few compact and open starting structures are considered. For $N = 7$, the topologies include bicapped trigonal bipyramid (BCTBP), capped octahedra (CO), and pentagonal bipyramid (PBP), while for $N = 8$, they are the tricapped trigonal bipyramid (TCTBP), bicapped octahedra (BCO), capped pentagonal bipyramid (CPBP), and cube (C). This choice is motivated by previous results for pure clusters and by the trend to compact geometries observed for smaller sizes $N \leq 6$. Although far from exhaustive, the considered geometries allow to explore various relevant growth patterns with a reasonable computational effort. Certainly, a more complete study would be necessary in order to draw definitive conclusions about the optimal topologies. For each composition, all possible distributions of the Fe and Rh atoms within the cluster, as well as all relevant values of the total magnetization S_z are taken into account (from the non-magnetic state to saturation). Therefore, the trends on the interplay between chemical order and magnetic behavior remain rigorous within the framework of the sampled topologies.

The results for $N = 7$ are summarized in Table VI. As in smaller Fe_mRh_n the binding energy per atom increases first with increasing Rh content and becomes essentially independent of composition in the Rh-rich limit ($5 \leq n \leq 7$). For pure Rh_7 the PBP is the most stable structure among the considered starting geometries. This result is consistent with some earlier DFT studies.⁵⁴ However it contrasts with the calculations by Wang *et al.*,⁶¹ who used the GGA functional of Ref. 34 (PW91) and obtained a capped octahedra, and with the calculations of Bae *et al.*,⁶² who found a prism plus an atom on a square face. According to

TABLE VI. (Color online) Structural, electronic and magnetic properties of FeRh heptamers as obtained from a restricted representative sampling of cluster topologies (see text).

Cluster	Struct.	E_B	ΔE_m	$d_{\alpha\beta}$	$\bar{\mu}_N$	μ_{Fe}	μ_{Rh}	ν_0
Fe ₇		2.95	0.84	2.47	3.14	2.88		209
Fe ₆ Rh		3.11	0.78	2.51 2.43	3.00	2.98	1.17	226
Fe ₅ Rh ₂		3.25	0.73	2.45 2.46	2.86	3.12	1.19	236
Fe ₄ Rh ₃		3.36	0.62	2.42 2.55 2.71	2.71	3.27	1.26	222
Fe ₃ Rh ₄		3.38	0.57	2.48 2.37 2.67	2.28	3.25	1.16	218
Fe ₂ Rh ₅		3.41	0.45	2.40 2.62	2.14	3.34	1.33	205
FeRh ₆		3.37	0.28	2.52 2.57	1.71	3.20	1.29	220
Rh ₇		3.33	0.22	2.61	1.86		1.62	203

our results, these structures are, respectively 20 and 4 meV per atom higher in energy than the PBP. In the case of a prism plus an atom on the square face, the energy difference with the ground state seems too small to be able to draw definitive conclusions.

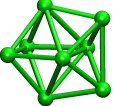
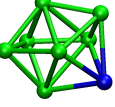
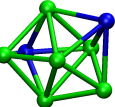
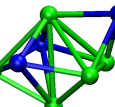
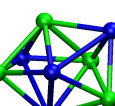
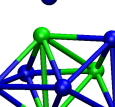
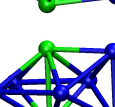
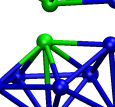
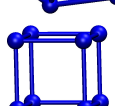
FeRh heptamers with high Rh concentrations also favor a PBP topology. In FeRh₆ the Fe atom occupies an apex site, while in Fe₂Rh₅ and Fe₃Rh₄ the Fe atoms belong to the pentagonal ring. Notice that the distances between the two apex atoms in Rh₇ and between the Fe and Rh apex atoms in FeRh₆ are relatively short. In Fe₂Rh₅ and Fe₃Rh₄ the Fe atoms are as far as possible from each other and the distance between the Rh apex atoms is larger. This is consistent with the previously discussed trend to favor the stronger FeRh bonds. For example, the energy involved in changing the position of the Fe atom in FeRh₆

from the apex (7 FeRh bonds) to the pentagonal ring (5 FeRh bonds) is 0.016 eV per atom.

As the Fe content increases, the topology of Fe_mRh_n changes. In fact Fe_4Rh_3 corresponds to a CO, while for $m \geq 5$ the configuration yielding the lowest energy can be regarded as a strongly distorted PBP (see Table VI). Already in Fe_4Rh_3 , but also in Fe_5Rh_2 , one observes a tendency of the Fe atoms to group in subclusters, bringing the Rh atoms to outer positions, so that the number of FeRh bonds is largest. Concerning the shape of the Fe rich heptamers, one observes important deformations of the pentagonal bipyramid (D_{5h} symmetry) which are similar to the distortions found in pure Fe_7 .^{63,64} While the precise origin of the symmetry lowering is difficult to establish in the alloys, it is reasonable to expect that it is similar to the case of pure Fe_7 . According to Ref. 64, the deformations found in Fe_7 are due to the presence of degenerate electronic states in the undistorted PBP structure. In order to verify this hypothesis we have analyzed the Kohn-Sham spectrum of the symmetric structure (D_{5h} symmetry) and found that it is highly degenerate at ε_F . In contrast the spectrum of the distorted structure has a band gap about 0.4 eV at ε_F . This suggests that the distortions in Fe rich FeRh clusters can be interpreted as a Jahn-Teller effect.

In Table VII results for FeRh octamers are reported. The general trends concerning the composition dependence of the binding energy, chemical order, as well as the average and local magnetic moments are very similar to smaller clusters. The most stable structure that we obtain for Fe_8 is a BCO having $E_B = 3.03$ eV, an average magnetic moment $\bar{\mu}_8 = 3\mu_B$, and a relatively short average bond-length $d = 2.42$ Å (see Table VII). A similar structure is also found in previous spin-polarized LDA calculations, where $E_B = 4.12$ eV and $\bar{\mu}_8 = 3\mu_B$ were obtained.⁶⁵ We have repeated these calculation for the BCO structure with our computational parameters and atomic reference energies and found $E_B = 3.51$ eV. The discrepancies between LDA and GGA results reflect the importance of exchange and correlation to the binding energy. In the other extreme, for pure Rh_8 , the structure that we find with the considered starting topologies is a regular cube having $E_B = 3.59$ eV, an average magnetic moment $\bar{\mu}_8 = 1.5\mu_B$, and all bond lengths equal to 2.40 Å. These results are in good agreement with previous calculations by Bae *et al.*⁶⁸ It is interesting to observe that the substitution of a single Rh atom by Fe in FeRh_7 results in a compact topology, which is more stable than the relatively open (relaxed) cube-like structures derived from pure Rh_8 . The same trend holds for higher Fe content (i.e., $\text{Fe}_m\text{Rh}_{8-m}$ with $m \geq 1$). The dominant structure for non-vanishing Fe content is a BCO with slight distortions. Only for

TABLE VII. (Color online) Structural, electronic and magnetic properties of FeRh octamers as obtained from a restricted representative sampling of cluster topologies (see text).

Cluster	Struct.	E_B	ΔE_m	$d_{\alpha\beta}$	$\bar{\mu}_N$	μ_{Fe}	μ_{Rh}	ν_0
Fe ₈		3.03	0.76	2.42	3.00	2.77		209
Fe ₇ Rh		3.19	0.73	2.43 2.47	2.87	2.88	1.04	208
Fe ₆ Rh ₂		3.32	0.66	2.43 2.47	2.75	3.18	1.04	190
Fe ₅ Rh ₃		3.42	0.69	2.43 2.57	2.62	3.15	1.10	189
Fe ₄ Rh ₄		3.47	0.53	2.45 2.42 2.70	2.50	3.20	1.25	197
Fe ₃ Rh ₅		3.54	0.42	2.77 2.39 2.65	2.37	3.36	1.34	214
Fe ₂ Rh ₆		3.53	0.32	2.70 2.59 2.57	2.00	3.25	1.30	208
FeRh ₇		3.49	0.23	2.45 2.57	1.62	3.27	1.18	202
Rh ₈		3.59	0.09	2.40	1.50		1.33	160

Fe₅Rh₃ we find a different topology, namely, a distorted CPBP. The typical isomerization energies between the BCO and the TCTBP are $\Delta E_{\text{iso}} = 10\text{--}30$ meV per atom. The average magnetic moments in the lowest lying isomers are either the same or very similar.

The magnetic properties of heptamers and octamers follow qualitatively the behavior observed in smaller clusters. In most cases the average magnetic moment per atom $\bar{\mu}_N$ and the magnetic energy ΔE_m increase with Fe concentration. The only exception is the pure Rh heptamer, for which $\bar{\mu}_7$ is somewhat larger than in FeRh₆. This is not due to AF-like coupling between Fe impurity moment and the remaining Rh atoms but rather to a

reduction of the Rh local moments in FeRh₆ ($\mu_i^{\text{Rh}} \simeq 1.61\text{--}1.63\mu_B$ in Rh₇, while $\mu_i^{\text{Rh}} \simeq 1.25\text{--}1.30\mu_B$ in FeRh₆). Remarkably, the Rh local moments in Rh₇ are the largest among all the heptamers. They amount to 87% of the total moment, which stresses the importance of the local *d*-electron contributions. Also in Rh₈ one finds quite large local moments, which are actually larger than the Rh moments in most Fe doped clusters. This shows that for these sizes the Fe atoms do not necessarily increase the Rh moments by simple proximity effects (see Tables VI and VII). Nevertheless, a different behavior is expected for larger *N*, where pure Rh clusters are no longer magnetic on their own. The local Fe moments are strongly enhanced with respect to pure Fe_{*N*} ($\mu_{\text{Fe}} \simeq 2.8\mu_B$ in Fe₇ or Fe₈) reaching values up to $3.36\mu_B$, particularly when the Fe atoms are in a Rh rich environment. As in the smaller clusters, this is a consequence of a charge transfer from the Fe to the Rh atoms, which increases the number of polarizable Fe *d*-holes. Notice that some kind of interaction between the Fe atoms seems to favor this effect, since the largest μ_{Fe} are found for clusters having 2 or 3 Fe atoms rather than for the single Fe impurity. Large Fe moments are also found in bulk FeRh alloys.^{14,66}

To conclude this section it is interesting to compare the cluster results with available experiments and calculations for macroscopic alloys.^{14,66,67} Band structure calculations for the periodic Fe_{0.5}Rh_{0.5} alloy having a CsCl structure yield an antiferromagnetic (AF) ground state, which is more stable than the ferromagnetic solution.⁶⁷ This is qualitatively in agreement with experiments showing AF order when the Rh concentration is above or equal to 50%.⁶⁶ In contrast our results for small clusters show a FM-like order for all Rh concentrations, even for the pure Rh clusters. This is a consequence of the reduction of local coordination number and the associated effective *d*-band narrowing, which renders the Stoner criterion far easier to satisfy, and which tends to stabilize the high-spin states with respect to the low-spin AF states. In fact, even in the bulk calculations on FeRh, the energies of the AF and FM states are not very different, and a coexistence of both solutions is found over a wide range of volumes.⁶⁷ Moreover, experiment shows an AF to FM transition with increasing temperature, which is accompanied by an enhanced thermal expansion.⁶⁶ Recent *ab initio* calculations have revealed the importance of competing FM and AF exchange interactions in stoichiometric α -FeRh.¹⁴ Moreover, neutron diffraction experiments⁶⁶ on Fe_{1-x}Rh_x for $0.35 < x < 0.5$ and calculations¹⁴ for $x = 0.5$ show that the Fe moments μ_{Fe} are significantly enhanced with respect to μ_{Fe} in pure α -Fe, particularly in the FM state where it reaches

values of about $3.2\mu_B$.^{14,66} These bulk results are remarkably similar to the trends found in Fe_mRh_n clusters over a wide range of compositions. As in the clusters, the induced Rh moments μ_{Rh} play an important role in the stability of the FM phase. Bulk experiments⁶⁶ on $\text{Fe}_{1-x}\text{Rh}_x$ yield $\mu_{\text{Rh}} \simeq 1\mu_B$ for $0.35 < x < 0.5$ which is comparable to, though somewhat smaller than the present cluster results.

IV. SIZE AND COMPOSITION DEPENDENCE

The main purpose of this section is to focus on the dependence of the electronic and magnetic properties of Fe_mRh_n clusters as a function of size and composition. In the following we present and discuss results for the binding energy, average and local spin moments, and electronic densities of states for $N = m + n \leq 8$.

A. Binding energy and magnetic moments

In Fig. 1 the binding energy per atom E_B is given as a function of the number of Fe atoms m . Besides the expected monotonic increase of E_B with increasing N , an interesting concentration dependence is observed. For very small sizes ($N \leq 4$) E_B is maximal for $m = 1$ or 2 , despite the fact that E_B is always larger for pure Rh than pure Fe clusters. This indicates that in these cases the bonding resulting from FeRh pairs is stronger than RhRh bonds. Only for $m \geq N - 1$, when the number of weaker FeFe bonds dominates, one observes that E_B decreases with increasing m . For larger sizes ($N \geq 5$) the strength of RhRh and FeRh bonds becomes very similar, so that the maximum in E_B is replaced by a range of Fe concentrations $x = m/N \lesssim 0.5$ where E_B depends very weakly on m .

In Fig. 2 the average magnetic moments $\bar{\mu}_N$ of Fe_mRh_n are shown as a function of m for $N \leq 8$. As already discussed in previous sections, $\bar{\mu}_N$ increases monotonously, with the number of Fe atoms. This is an expected consequence of the larger Fe local moments and the underlying FM-like magnetic order. The average slope of the curves tends to increase with decreasing N , since the change in concentration per Fe substitution is more important the smaller the size is. The typical increase in $\bar{\mu}_N$ per Fe substitution is about $(1/N)\mu_B$ per Fe substitution. Notice, moreover, the enhancement of the magnetic moments of the pure clusters in particular for Fe_N ($m = N$), which go well beyond $3\mu_B$, the value corresponding

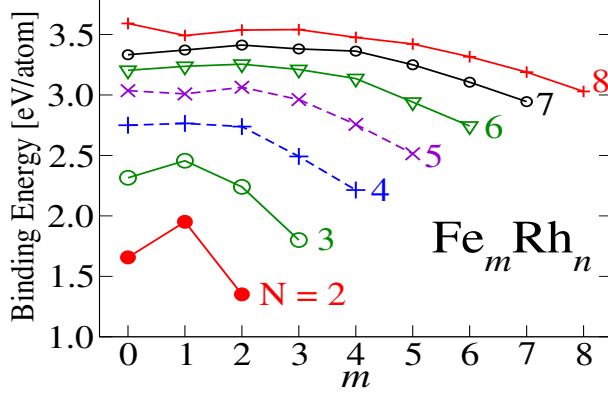


FIG. 1. (Color online) Binding energy per atom E_B of Fe_mRh_n clusters as a function of the number of Fe atoms. The lines connecting the points for each $N = m + n$ are a guide to the eye.

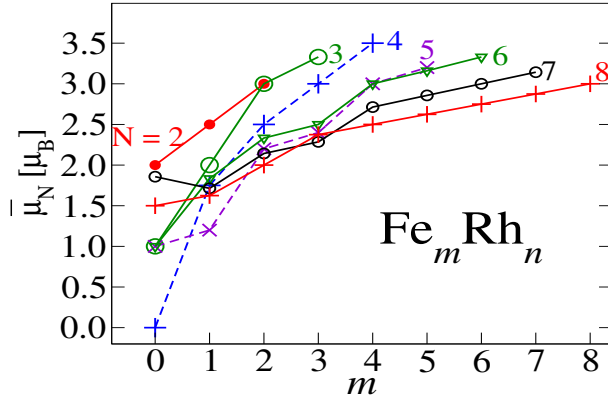


FIG. 2. (Color online) Total magnetic moment per atom $\bar{\mu}_N$ of Fe_mRh_n clusters as a function of number of Fe atoms. The symbols corresponding to each size are the same as in Fig. 1. The lines connecting the points for each $N = m + n$ are a guide to the eye.

to a saturated d -band in the d^7s^1 configuration. In contrast, the moments of pure Rh_N are far from saturated except for $N = 2$ and 7 (see Fig. 2 for $m = 0$). In this context it is important to recall that a thorough global optimization, for example, by considering a large number of initial topologies, could affect the quantitative values of the magnetic moments for $N = 7$ and 8 .

The local magnetic moments in the PAW sphere of the Fe and Rh atoms provide further insight on the interplay between $3d$ and $4d$ magnetism in Fe_mRh_n . In Fig. 3 μ_{Fe} and μ_{Rh} are shown as a function of m for $N = 6-8$. The Fe moments are essentially given by the saturated d -orbital contribution. For pure Fe clusters the actual values of μ_{Fe} within the

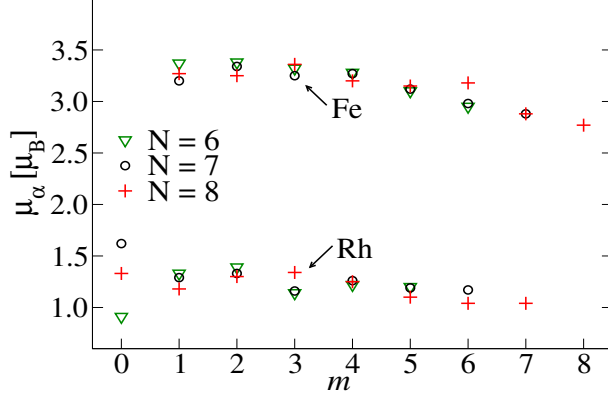


FIG. 3. (Color online) Local magnetic moment μ_α at the Fe and Rh atoms as a function of the number Fe atoms m .

PAW sphere are somewhat lower than $3\mu_B$ due to a partial spill-off of the spin-polarized density. Notice that the Fe moments increase as we replace Fe by Rh atoms showing some weak oscillations as a function of m . The increase is rather weak for a single Rh impurity in Fe_{N-1}Rh but becomes stronger reaching a more or less constant value as soon as the cluster contains 2 or more Rh ($m \leq N - 2$, see Fig. 3). This effect can be traced back to a d electron charge transfer from Fe to Rh which, together with the extremely low coordination number, yields a full polarization of the larger number of Fe d holes. On the other side the Rh moments are not saturated and therefore are more sensitive to size, structure and composition. The values of μ_{Rh} are in the range of $1-1.5\mu_B$ showing some oscillations as a function of m . No systematic enhancement of μ_{Rh} with increasing Fe content is observed. This behavior could be related to charge transfers effects leading to changes in the number of Rh d electrons as a function of m .

Finally, it is interesting to analyze the role played by magnetism in defining the cluster structure by comparing magnetic and non-magnetic calculations. For the smallest FeRh clusters ($N = 3$ and 4) the magnetic energy $\Delta E_m = E(S_z = 0) - E(S_z)$ gained upon magnetization is higher in the first excited isomer than in the most stable structure. This implies that the contribution of magnetism to the structural stability is not crucial, since the non-magnetic calculations yield the same ordering, at least concerning the two best structures. This suggests that for the smallest sizes the kinetic or bonding energy dominates the structural stability, which also explains that the two most stable isomers have different topologies. The situation changes for large clusters. For $N \geq 5$ one finds a number of FeRh

clusters for which the optimal structure is actually stabilized by magnetism. For example, in Fe_4Rh , Fe_3Rh_2 , and FeRh_4 the energy ordering of the two most stable isomers would be reversed if magnetism were neglected. It should be noted that in these cases the structures differ only in the chemical order, not in the topology which is a TBP. In the FeRh hexamers the energy differences between the low-lying isomers are more important and only in one case, Fe_4Rh_2 , magnetism appears to be crucial for stabilizing the actual optimal structure. A similar strong interplay between structure, chemical order and magnetism is expected for larger FeRh clusters.

B. Electronic structure

In the previous sections the structure and spin moments of FeRh alloy clusters have been discussed as a function of $3d/4d$ concentration. Although these properties are intimately related to the size and composition dependence of electronic structure, it is in general very difficult to achieve a physical transparent correlation between global and microscopic behaviors. Nevertheless, it is very interesting to analyze, at least for some representative examples, how the electronic structure depends on the composition of magnetic nanoalloys. To this aim we report in Fig. 4 the spin-polarized d -electron density of states (DOS) of representative FeRh octamers having the relaxed structures illustrated in Table VII. Results for pure Fe_8 and Rh_8 are also shown for the sake of comparison. In all the clusters, the dominant peaks in the relevant energy range near ε_F correspond either to the Fe- $3d$ or to the Rh- $4d$ states. The valence spectrum is largely dominated by these d -electron contributions. In fact the total DOS and the d -projected DOS are difficult to tell apart.

First of all, let us consider the DOS of the pure clusters. Our results for Rh_8 with a cube structure are similar to those of previous studies.⁶⁸ They show the dominant d -electron contribution near ε_F , with the characteristic ferromagnetic exchange splitting between the minority and majority spin states. In Fig. 4 we also included the DOS for Rh_8 with a BCO structure, since it allows us to illustrate the differences in the electronic structure of compact and open geometries. Moreover, the DOS of pure Rh_8 with BCO structure is very useful in order to demonstrate the dependence of DOS on Fe content, since the structures of $\text{Fe}_m\text{Rh}_{8-m}$ with $m \geq 1$ are similar to the BCO. Both Fe_8 and Rh_8 show relatively narrow d -bands which dominate the single-particle energy spectrum in the range

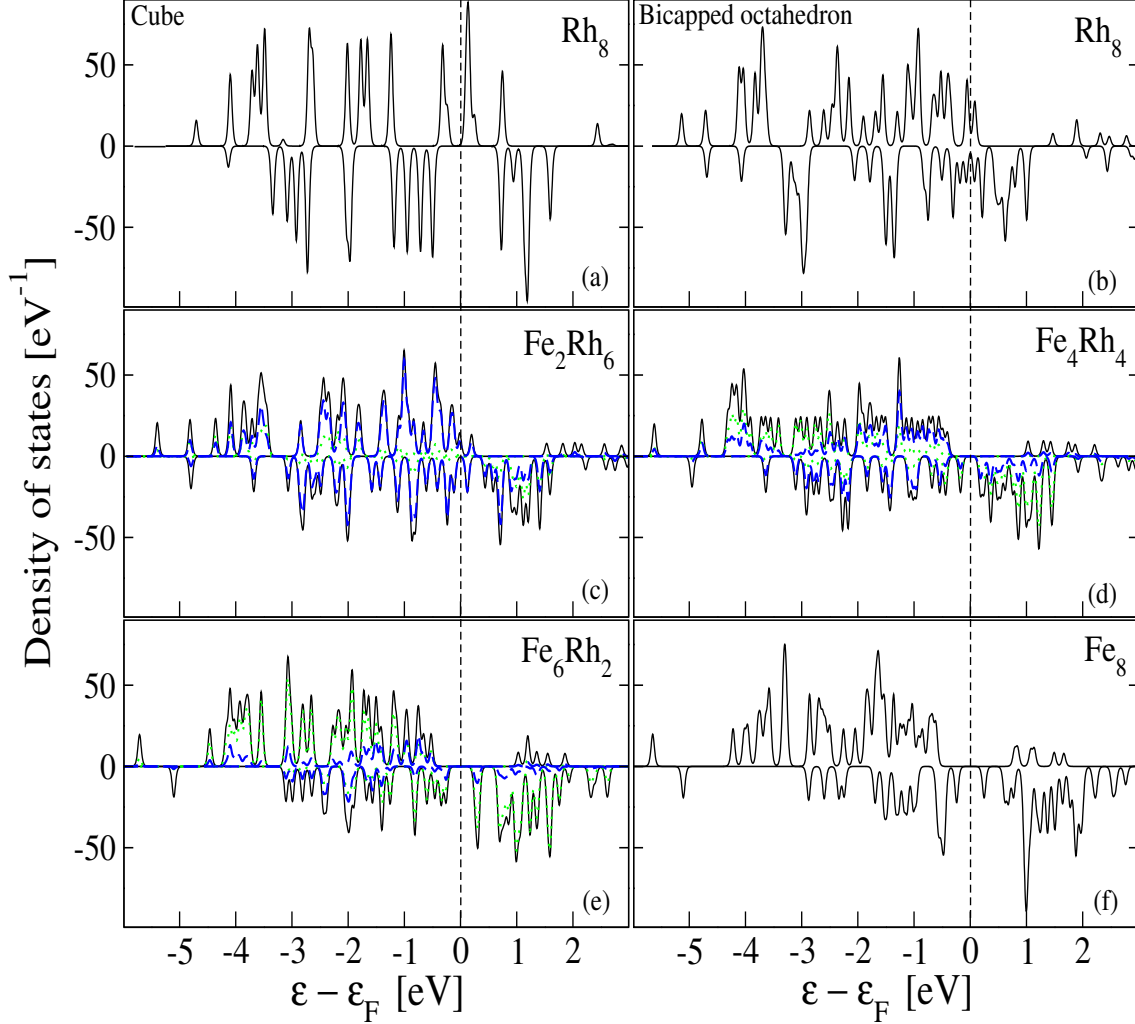


FIG. 4. (Color online) Electronic density of states (DOS) of FeRh octamers. Results are given for the total (solid), the Fe-projected (dotted), and the Rh-projected (dashed) d -electron DOS. Positive (negative) values correspond to majority (minority) spin. A Lorentzian width $\lambda = 0.02$ eV has been used to broaden the discrete energy levels. The corresponding structures are illustrated in Table VII.

$-5\text{eV} \leq \varepsilon - \varepsilon_F \leq 3\text{eV}$. The spin polarization of the DOS clearly reflects the ferromagnetic order in the cluster. Putting aside the exchange splitting, the peak structure in the up and down DOS $\rho_\sigma(\varepsilon)$ are comparable. There are even qualitative similarities between the two elements. However, looking in more detail, one observes that the effective d -band width in Fe_8 (about 4 eV) is somewhat smaller than in Rh_8 (about 5 eV). Moreover, in Rh_8 the DOS at ε_F is non-vanishing for both spin directions and the finite-size gaps are very small (see Fig. 4). In contrast, the majority d -DOS is fully occupied in Fe_8 , with the highest majority

state lying about 0.5 eV below ε_F . In addition there is an appreciable gap (about 0.1 eV) in the corresponding minority spectrum. These qualitative differences are of course consistent with the fact that Fe_8 is a strong ferromagnet with saturated moments, while Rh_8 should be regarded as a weak unsaturated ferromagnet.

The trends as a function of concentration reflect the crossover between the previous contrasting behaviors. For low Fe concentration (e.g., Fe_2Rh_6) we still find states with both spin directions close to ε_F . The magnetic moments are not saturated, although the Fermi energy tends to approach the top of the majority band. Moreover, the majority-spin states close to ε_F have dominantly Rh character. Small Fe doping does not reduce the d -band width significantly. Notice the rather important change in the shape of the DOS in Fe_2Rh_6 as compared to the DOS in Rh_8 . This is a consequence of the change in topology from cubic to bicapped octahedron (BCO).

For equal concentrations (Fe_4Rh_4) the first signs of d -band narrowing and enhanced exchange splitting start to become apparent. The spin-up states (majority band) which in Fe_2Rh_6 contribute to the DOS at ε_F now move to lower energies (0.3 eV below ε_F) so that the majority band is saturated. Only spin-down (minority) states are found around ε_F , although there is a significant gap in $\rho_{\downarrow}(\varepsilon)$ (see Fig. 4). In the majority band Rh dominates over Fe at the higher energies (closer to ε_F), while Fe dominates in the bottom of the band. In the minority band the participation of Rh (Fe) is stronger (weaker) below ε_F and weaker (stronger) above ε_F . This is consistent with the fact that the Rh local moments are smaller than the Fe moments.

Finally, in the Fe rich limit (e.g., Fe_6Rh_2), the majority-band width becomes as narrow as in Fe_8 , while the minority band is still comparable to Rh_8 . The exchange splitting is large, the majority band saturated and only minority states are found close to ε_F . As in Fe_8 , $\rho_{\downarrow}(\varepsilon)$ shows a clear gap at ε_F (see Fig. 4). However, the Rh contribution to the minority states below ε_F remains above average despite the relative small Rh content. The Fe contribution largely dominates the unoccupied minority-spin DOS, in agreement with the larger local Fe moments.

V. DISCUSSION

The structural, electronic and magnetic properties of small Fe_mRh_n clusters having $N = m + n \leq 8$ atoms have been investigated systematically in the framework of a generalized gradient approximation to density-functional theory. For very small sizes ($N \leq 4$ atoms) the binding energy E_B shows a non-monotonous dependence on concentration, which implies that the FeRh bonds are stronger than the homogeneous ones. However, for larger sizes the FeRh and RhRh bond strengths become comparable, so that E_B depends weakly on concentration for high Rh content.

The magnetic order of the clusters having the most stable structures is found to be FM-like. Moreover, the average magnetic moment per atom $\bar{\mu}_N$ increases monotonously, which is almost linear over a wide range of concentration with Fe content. Consequently, the energy gain ΔE_m associated to magnetism also increases with the number of Fe atoms. The largest part of the spin polarization (about 90%) can be traced back to the local d magnetic moments within the PAW sphere of the atoms. The s and p spin polarizations are almost negligible in general. A remarkable enhancement of the local Fe moments is observed as result of Rh doping. This is a consequence of the increase in the number of Fe d holes, due to charge transfer from Fe to Rh, combined with the extremely reduced local coordination. The Rh local moments are important already in the pure clusters ($N \leq 8$). Therefore, they are not significantly enhanced by Fe doping. However, the overall stability of magnetism, as measured by the total energy gained by the onset of spin polarization, is found to increase with increasing Fe content.

A further interesting aspect, particularly for future studies is the role of spin-orbit (SO) interactions on the magnetism of nanoalloys. We have performed some representative calculations by taking into account spin-orbit coupling (SOC) in order to explore their effect on the ground-state structure, chemical order and spin moments. For example in Fe_6 , Fe_3Rh_3 and Rh_6 we find that the changes in the ground-state energy resulting from SO interaction are typically of the order of 0.2 eV for the whole cluster. This is often comparable to or larger than the energy differences between the low-lying isomers. However, the SO energies are very similar for different structures, so that the ground-state structures remain essentially the same as in the scalar relativistic (SR) calculations. The changes in the bond lengths and in the spin moments resulting from SOC are also very small (e.g., $|\bar{\mu}^{\text{SOC}} - \bar{\mu}^{\text{SR}}| \simeq 0.01\mu_B$

and $|d_{ij}^{\text{SOC}} - d_{ij}^{\text{SR}}| \simeq 0.001\text{\AA}$ in Fe_3Rh_3). As a result, the conclusions drawn from our SR calculations on the relative stability and local spin moments seem to be unaffected by the spin-orbit contributions.

FeRh clusters are expected to develop a variety of further interesting behaviors, which still remain to be explored. For instance, larger cluster should show a more complex dependence of the magnetic order as a function of concentration. In particular for large Rh content one should observe a transition from FM-like to AF-like order with increasing cluster size, in agreement with the AF phase found in solids for more than 50% Rh concentration. Moreover, the metamagnetic transition observed in bulk FeRh alloys also puts forward the possibility of similar interesting phenomena in nanoalloys as a function of temperature. Finally, the contributions of orbital magnetism and magnetic anisotropy deserve to be explored in detail as a function of composition and chemical order, even for the smallest sizes, particularly because of their implications for potential applications.⁶⁹

ACKNOWLEDGMENTS

It is pleasure to thank Dr. J. L. Ricardo-Chávez and Dr. L. Díaz-Sánchez for helpful discussions and useful comments. Computer resources from ITS (Kassel) and CSC (Frankfurt) are gratefully acknowledged.

-
- ¹ See, for instance, Faraday Discuss. **138** (2008).
 - ² D. Zitoun, M. Respaud, M. C. Fromen, M. J. Casanove, P. Lecante, C. Amiens, and B. Chaudret, Phys. Rev. Lett. **89**, 037203 (2002).
 - ³ S. Dennler, J. L. Ricardo-Chávez, J. Morillo, and G. M. Pastor, Eur. Phys. J. D **24**, 237 (2003).
 - ⁴ I. Efremenko, and M. Sheintuch, Chem. Phys. Lett. **401**, 232-240 (2005).
 - ⁵ S. Ganguly, M. Kabir, S. Datta, B. Sanyal, and A. Mookerjee, Phys. Rev. B. **78**, 014402 (2008).
 - ⁶ P. Entel, and M. E. Gruner, J. Phys. Condens. Matter **21**, 064228 (2009).
 - ⁷ A. N. Andriotis, G. Mpourmpakis, G. E. Froudakis, and M. Menon, J. Chem. Phys. **120**, 11901 (2004).
 - ⁸ G. Rollmann, S. Sahoo, A. Hucht, and P. Entel, Phys. Rev. B **78**, 134404 (2008).

- ⁹ J. Bansmann, S. Baker, C. Binns, J. Blackman, J.-P. Buecher, J. Dorantes-Dávila, V. Dupuis, L. Favre, D. Kechrakos, A. Kleibert, K.-H. Meiwes-Broer, G. M. Pastor, A. Perez, O. Toulemonde, K.N. Trohidou, J. Tuaille, and Y. Xie, *Surf. Sci. Rep.* **56**, 189 (2005).
- ¹⁰ C. Antoniak, J. Lindner, M. Spasova, D. Sudfeld, M. Acet, M. Farle, K. Fauth, U. Wiedwald, H.-G. Boyen, P. Ziemann, F. Wilhelm, A. Rogalev, and S. Sun, *Phys. Rev. Lett.* **97**, 117201 (2006).
- ¹¹ S. Yin, R. Moro, X. Xu, and W. A. de Heer, *Phys. Rev. Lett.* **98**, 113401 (2007).
- ¹² M. B. Knickelbein, *Phys. Rev. B* **75**, 014401 (2007).
- ¹³ R. M. Wang, O. Dmitrieva, M. Farle, G. Dumpich, H. Q. Ye, H. Poppa, R. Kilaas, and C. Kisielowski, *Phys. Rev. Lett.* **100**, 017205 (2008).
- ¹⁴ M. E. Gruner, G. Rollmann, P. Entel, and M. Farle *Phys. Rev. Lett.* **100**, 087203 (2008).
- ¹⁵ Yan Sun, Min Zhang, and René Fournier, *Phys. Rev. B* **77**, 075435 (2008).
- ¹⁶ Yan Sun, René Fournier, and Min Zhang, *Phys. Rev. A* **79**, 043202 (2009).
- ¹⁷ F. Tournus, A. Tamion, N. Blanc, A. Hannour, L. Bardotti, B. Prével, P. Ohresser, E. Bonet, T. Epicier, and V. Dupuis, *Phys. Rev. B* **77**, 144411 (2008).
- ¹⁸ G. M. Pastor, J. Dorantes-Dávila, and K. H. Bennemann, *Physica B* **149**, 22 (1988); *Phys. Rev. B* **40**, 7642 (1989).
- ¹⁹ J. P. Bucher, D. C. Douglass, and L. A. Bloomfield *Phys. Rev. Lett.* **66**, 3052 (1991); D. C. Douglass, J. P. Bucher, and L. A. Bloomfield, *Phys. Rev. B* **45**, 6341 (1992); D. C. Douglass, A. J. Cox, J. P. Bucher, and L. A. Bloomfield, *ibid.* **47**, 12874 (1993).
- ²⁰ I. M. L. Billas, J. A. Becker, A. Chatelain, and W. A. de Heer, *Phys. Rev. Lett.* **71**, 4067 (1993); I. M. L. Billas, A. Châtelain, and W. A. de Heer, *Science* **265**, 1682 (1994).
- ²¹ G. M. Pastor, J. Dorantes-Dávila, S. Pick, and H. Dreyssé, *Phys. Rev. Lett.* **75**, 326 (1995).
- ²² S. E. Apsel, J. W. Emmert, J. Deng, and L. A. Bloomfield, *Phys. Rev. Lett.* **76**, 1441 (1996).
- ²³ M. B. Knickelbein, *Phys. Rev. Lett.* **86**, 5255 (2001).
- ²⁴ G. Nicolas, J. Dorantes-Dávila, and G.M. Pastor, *Phys. Rev. B* **74**, 014415 (2006).
- ²⁵ R. Galicia, *Rev. Mex. Fis.* **32**, 51 (1985).
- ²⁶ J. Dorantes-Dávila, H. Dreyse, and G. M. Pastor, *Phys. Rev. B* **46**, 10432 (1992).
- ²⁷ A. J. Cox, J. G. Louderback, and L. A. Bloomfield, *Phys. Rev. Lett.* **71**, 923 (1993); A. J. Cox, J. G. Louderback, S. E. Apsel, and L. A. Bloomfield, *Phys. Rev. B* **49**, 12295 (1994).
- ²⁸ B. V. Reddy, S. N. Khanna, and B. I. Dunlap, *Phys. Rev. Lett.* **70**, 3323 (1993).

- ²⁹ P. Villaseñor-González, J. Dorantes-Dávila, H. Dreyssé, and G. M. Pastor, *Phys. Rev. B* **55**, 15084 (1997).
- ³⁰ P. Hohenberg and W. Kohn, *Phys. Rev.* **136**, B864 (1964); W. Kohn and L. J. Sham, *Phys. Rev.* **140**, A1133 (1965).
- ³¹ T. B. Massalski, J. L. Murray, L. H. Bennett, and H. Baker, *Binary Alloy Phase Diagrams*, Vol. 1, (American Society for Metals, Metals Park, OH, 1986).
- ³² M. E. Gruner, E. Hoffmann, and P. Entel, *Phys. Rev. B* **67**, 064415 (2003).
- ³³ G. Kresse and J. Furthmüller, *Phys. Rev. B* **54**, 11169 (1996); G. Kresse and D. Joubert, *Phys. Rev.* **59**, 1758 (1999).
- ³⁴ J. P. Perdew, J. A. Chevary, S. H. Vosko, K. A. Jackson, M. R. Pederson, D. J. Singh, and Carlos Fiolhais, *Phys. Rev. B* **46**, 6671 (1992).
- ³⁵ P. E. Blöchl, *Phys. Rev. B*, **50**, 17953 (1994).
- ³⁶ A number of tests have been performed in order to assess the numerical accuracy of the calculations. Increasing the cut-off energy $E_{max} = 268$ eV and supercell size $a = 12$ Å to $E_{max} = 500$ eV and $a = 22$ Å in Rh_4 increases the computation time by a factor 4–7. This yields a total energy differences of 1.75 meV and 0.25 meV, respectively. In the above calculations the changes in average bond length (bond angle) amounts to 10^{-3} Å (10^{-4} degrees). These difference are not significant for our physical conclusions. In fact, typical isomerization energies in these clusters are an order of magnitude larger, of the order of 10–30 meV. We also found that the total energy is nearly independent of the choice of the smearing parameter σ , provided it is not too large ($\sigma \leq 0.05$ eV). Values from $\sigma = 0.01$ to 0.1 eV have been checked. Therefore, we judge that our set of standard parameters ($E_{max} = 268$ eV, supercell size a from 10 to 22 Å, and $\sigma = 0.02$ eV) offers a sufficiently good accuracy at a reasonable computational costs.
- ³⁷ M. Muñoz-Navia, J. Dorantes-Dávila, D. Zitoun, C. Amiens, B. Chaudret, M.-J. Casanove, P. Lecante, N. Jaouen, A. Rogalev, M. Respaud, and G. M. Pastor, *Faraday Discuss.* **138**, 181 (2008); M. Muñoz-Navia, J. Dorantes-Dávila, M. Respaud, and G. M. Pastor, *Eur. J. Phys. D* **52**, 171 (2009).
- ³⁸ G. M. Pastor, R. Hirsch, and B. Mühlshlegel, *Phys. Rev. Lett.* **72**, 3879 (1994); *Phys. Rev. B* **53**, 10382 (1996).
- ³⁹ R. Garibay-Alonso, J. Dorantes-Dávila, and G. M. Pastor, *Phys. Rev. B* **79**, 134401 (2009).
- ⁴⁰ Results for lower lying isomers and excited magnetic configurations will be reported elsewhere.

- ⁴¹ Y. Wang, T. F. George, D. M. Lindsay, and A. C. Beri, *J. Chem. Phys.* **86**, 3493 (1987).
- ⁴² The precise choice of the NN distances is not very important, since this concerns merely the configuration for starting the unconstrained structural relaxation.
- ⁴³ G. Kresse and Jürgen Furthmüller, *VASP The Guide*, <http://cms.mpi.univie.ac.at/vasp>.
- ⁴⁴ For a discussion of the interplay between electron correlations, structure and magnetism of small clusters see, for example, Refs. 18 and 38.
- ⁴⁵ R.F.W. Bader, *Atoms in Molecules, A Quantum Theory* (Oxford University Press, Oxford, 1990).
- ⁴⁶ J.L. Ricardo-Chávez, PhD Thesis, Université Paul Sabatier, Toulouse, France, (2007).
- ⁴⁷ G. L. Gutsev, S. N. Khanna, and P. Jena, *Phys. Rev. B* **62**, 1604 (2000); S. Chrétien and D. R. Salahub, *Phys. Rev. B* **66**, 155425 (2002); G. Rollmann and P. Entel, *Computing Letters (CoLe)*, Vol. 1, No. 4, 288-296 (2004).
- ⁴⁸ M. Castro, and D. R. Salahub, *Phys. Rev. B* **49**, 11842 (1994); L. Wang, Q Ge, *Chem. Phys. Lett.* **366**, 368-376 (2002); C. H. Chien, E. Blaisten-Barojas, and M. R. Pederson, *Phys. Rev. A* **58**, 2196 (1998); J. L. Chen, C. S. Wang, K. A. Jackson, and M. R. Pederson, *Phys. Rev. B* **44**, 6558 (1991). D. M. Cox, D. J. Trevor, R. L. Whetten, E. A. Rohlfing, and A. Kaldor, *Phys. Rev. B* **32**, 7290 (1985).
- ⁴⁹ S. E. Apsel, J. W. Emmert, J. Deng, and L. A. Bloomfield, *Phys. Rev. Lett.* **76**, 1441 (1996).
- ⁵⁰ M. Castro, C. Jamorski, and D. R. Salahub, *Chem. Phys. Lett.* **271**, 133 (1997); S. E. Weber and P. Jena, *Chem. Phys. Lett.* **281**, 401 (1997); B. V. Reddy, S. K. Nayak, S. N. Khanna, B. K. Rao, and P. Jena, *J. Phys. Chem. A* **102**, 1748 (1998).
- ⁵¹ M. Moskovits and D. P. Dilella, *J. Chem. Phys.* **73**, 4917 (1980).
- ⁵² D. G. Leopold and W. C. Linenger, *J. Chem. Phys.* **85**, 51 (1986).
- ⁵³ B. V. Reddy, S. K. Nayak, S. N. Khanna, B. K. Rao, and P. Jena, *Phys. Rev. B* **59**, 5214 (1999).
- ⁵⁴ T. Futschek, M. Marsman, and J. Hafner, *J. Phys. C. M.* **17**, 5927 (2005).
- ⁵⁵ B. Delley, *J. Chem. Phys.* **92**, 508, (1990); **113**, 7756 (2000).
- ⁵⁶ D. L. Cocke and K. A. Gingerich, *J. Chem. Phys.* **60**, 1958 (1974).
- ⁵⁷ H. Wang, H. Haouari, R. Craig, Y. Lui, J. R. Lombardi, and D. M. Lindsay, *J. Chem. Phys.*, **106**, 2101 (1997).
- ⁵⁸ J. D. Langenberg and M. D. Morse, *J. Chem. Phys.*, **108**, 2331 (1998).
- ⁵⁹ L. Pauling, *J. Am. Chem. Soc.* **54**, 3570 (1932).

- ⁶⁰ The optimal Fe_3Rh_2 structure has 6 FeRh and 3 FeFe NN pairs, while the first isomer has 5 FeRh, 3 FeFe, and 1 RhRh NN pairs. The optimal Fe_2Rh_3 structure has 6 FeRh and 3 RhRh NN pairs, while the first isomer has 6 FeRh, 2 RhRh, and 1 FeFe NN pairs.
- ⁶¹ L. Wang and Q. Ge, Chem. Phys. Lett. **366**, 368-376 (2002).
- ⁶² Y.-C. Bae, H. Osanai, V. Kumar, and Y. Kawazoe, Phys. Rev. B **70**, 195413 (2004).
- ⁶³ P. Ballone and R. O. Jones, Chem. Phys. Lett. **233**, 632 (1995).
- ⁶⁴ G. Rollmann, P. Entel, and S. Sahoo, Comput. Mater. Sci. **35**, 275 (2005).
- ⁶⁵ O. Diéguez, M. M. G. Alemany, C. Rey, P. Ordejón, and L. J. Gallego, Phys. Rev. B **63**, 205407 (2001).
- ⁶⁶ G. Shirane and R. Nathans, Phys. Rev., **134**, A1547-A1553 (1964).
- ⁶⁷ V. L. Moruzzi and P. M. Marcus, Phys. Rev. B **46**, 2864 (1992).
- ⁶⁸ Y.-C. Bae, V. Kumar, H. Osanai, and Y. Kawazoe, Phys. Rev. B **72**, 125427 (2005).
- ⁶⁹ M. Muñoz-Navia, J. Dorantes-Dávila, D. Zitoun, C. Amiens, N. Jaouen, A. Rogalev, M. Respaud, and G. M. Pastor, Appl. Phys. Lett. **95**, 233107 (2009).